

# Analytical expressions for the longitudinal evolution of nondiffracting pulses truncated by finite apertures.

Michel Zamboni-Rached,

*D.M.O., Faculty of Electrical Engineering, UNICAMP, Campinas, SP, Brasil.*

## Abstract

In this paper, starting from some general and plausible assumptions based on geometrical optics and on a common feature of the truncated Bessel beams, a heuristic derivation is presented of very simple *analytical* expressions, capable of describing the longitudinal (on-axis) evolution of axially-symmetric nondiffracting pulses when truncated by finite apertures. We apply our analytical formulation to several situations involving subluminal, luminal or superluminal localized pulses, and compare the results with those obtained by numerical simulations of the Rayleigh-Sommerfeld diffraction integrals. The results are in excellent agreement. The present approach can be rather useful, because it yields, in general, closed-form expressions, avoiding the need of time-consuming numerical simulations; and also because such expressions provide a powerful tool for exploring several important properties of the truncated localized pulses, as their depth of fields, the longitudinal pulse behavior, the decaying rates, and so on.

*PACS nos.:* 41.20.Jb ; 03.50.De ; 03.30.+p ; 84.40.Az ; 42.82.Et ; 83.50.Vr ; 62.30.+d ; 43.60.+d ; 91.30.Fn ; 04.30.Nk ; 42.25.Bs ; 46.40.Cd ; 52.35.Lv .

*Keywords:* Localized solutions to Maxwell equations; Superluminal waves; Bessel beams; Limited-diffraction pulses; Finite-energy waves; Electromagnetic wavelets; X-shaped waves; Electromagnetism; Microwaves; Optics; Special relativity; Localized acoustic waves; Diffraction theory

## 1 Introduction

Ideal nondiffracting pulses (INP) are infinite energy solutions of the ordinary linear wave equation, capable of maintaining their spatial shapes indefinitely (sometimes with

just small local variations) while propagating[1-9]. When these ideal solutions are to be adapted to real situations and applications, they must be spatially truncated by a finite aperture (i.e., generated by a finite aperture), getting transformed into finite energy solutions, with finite field depths, even if these field-depths are very large when compared to those of ordinary pulses.

When we truncate an INP, the resulting wave field cannot be obtained, in general, in analytical form. In this case one has to resort to the diffraction theory and perform numerical simulations of the diffraction integrals, such as that, well known, of Rayleigh-Sommerfeld[10].

Indeed, one can get very important pieces of information about a truncated nondiffracting pulse (TNP) by performing numerical simulations of its longitudinal evolution[11-14], especially when the pulse is axially symmetric.

In this paper we shall show that, by using some general and plausible assumptions, based on geometrical optics and on a common feature of truncated Bessel beams, a heuristic derivation of simple analytical expressions is possible, capable of furnishing the longitudinal (on-axis) evolution of the TNPs. It is interesting to notice that this approach depends only on the spectral structure of the relevant INP.

We compare the results of our analytical method, when applied to several different situations involving subluminal, luminal or superluminal TNPs, with the results obtained from the usual numerical simulation of the Rayleigh-Sommerfeld integrals: the results are in an excellent agreement.

This method, due to its extreme simplicity and analytical character, can be a powerful tool for exploring several important properties of the TNPs, as their depth of fields, the longitudinal pulse behavior, the decaying rates, etc.; for revealing the effects of the spectral parameters on the pulses evolution; and also for comparing the “effectiveness” of the different kinds of TNPs, as the subluminal, luminal and superluminal ones. Without

this method, all those results could be reached (in each particular situation) only by performing several time-consuming numerical simulations.

## 2 Heuristic approach for describing the on-axis evolution of TNPs

Let us begin this Section by making some comments about the truncated Bessel beams and about some approximations, which will be used below for developing the method here proposed.

### 2.1 Some observations and approximations about truncated Bessel beams

An ideal (infinite energy) Bessel beam (IBb) is given by[15]

$$\Psi_{\text{IBb}}(\rho, z, t) = J_0(k_\rho \rho) e^{i\beta z} e^{-i\omega t} , \quad (1)$$

where  $\rho^2 = x^2 + y^2$  is the transverse coordinate,  $k_\rho^2 = \omega^2/c^2 - \beta^2$  is the transverse wavenumber,  $\beta$  is the longitudinal wavenumber, and  $\omega$  is the angular frequency.

An important parameter[16-19] of an IBb is its axicon angle  $\theta$ , where  $\omega = c\beta/\cos\theta$ .

When a Bessel beam is truncated by a finite aperture of radius  $R$ , Eq.(1) cannot be used to describe the resulting beam in the whole space. However, if the size of the aperture is big enough to contain several bright rings of the ideal incident Bessel beam, i.e., if  $R \gg 1/k_\rho$ , we can use geometrical optics to get some characteristics of the truncated Bessel beam (TBb) evolution.

In this case (see Fig.1), we can say that, in the spatial region localized inside the cone oriented along the  $z$ -axis, with apex at  $z = Z = R/\tan\theta$  and base given by the circular aperture, the resulting TBb can be approximately described by Eq.(1).

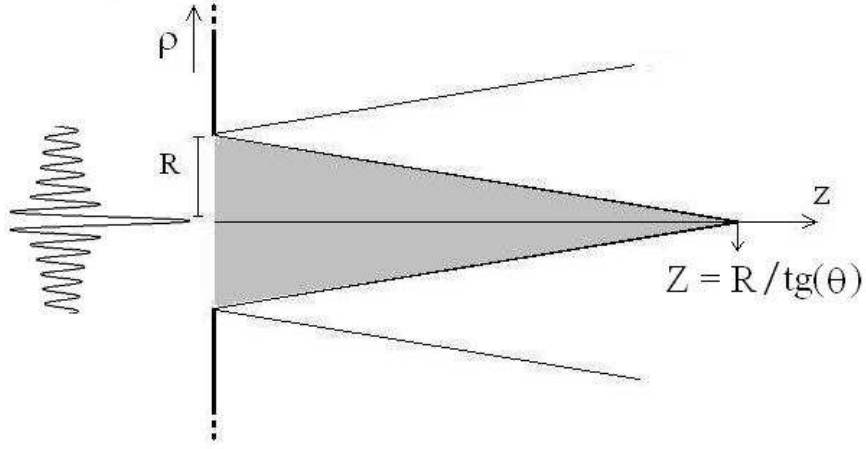


Figure 1: A typical Bessel beam truncated by a finite aperture.

However, when using geometrical optics, after the distance  $Z = R/\tan\theta$  the on-axis amplitude of the TBb becomes approximately zero (see Fig.1). The distance  $Z$  is called the depth-field of the TBb.

Keeping the above observations in mind, one may affirm that, since  $R \gg 1/k_\rho$ , the on-axis behavior of a TBb can be approximately described by

$$\Psi_{\text{TBb}}(\rho = 0, z, t) \simeq \begin{cases} e^{i\beta z} e^{-i\omega t} & \text{for } z \leq \frac{R}{\tan\theta} \\ 0 & \text{for } z > \frac{R}{\tan\theta} \end{cases} \quad (2)$$

which can be compactly written as

$$\Psi_{\text{TBb}}(\rho = 0, z, t) \simeq e^{i\beta z} e^{-i\omega t} \left[ H(z) - H\left(z - \frac{R}{\tan\theta}\right) \right] \quad (3)$$

where  $H(\cdot)$  is the Heaviside step function. *The equation above is the starting point for our heuristic method describing the on-axis TNP's behavior.*

According to the approximation Eq.(3), the on-axis field intensity of a TBb is a rectangular function with unitary value, till  $z = Z$ .

On the other hand, when a numerical simulation of the diffraction integrals is performed[8,15], one can observe that the TBb presents some on-axis field oscillations around the unitary value, before suffering an abrupt decay after  $z = Z$ . Such oscillations cannot be predicted by geometrical optics, and arise only due to the abrupt truncation made by the aperture. However, it is important to stress here that, despite the fact that those oscillations are not predicted by Eq.(3), such an error *is not present*, in general, in the case of our description of truncated localized pulses. One can understand this by noticing that, since nondiffracting pulses are constructed through Bessel beams superpositions, those oscillations, originating from each TBb, suffer a destructive interference.

With all this in mind, we are ready to develop our method.

## 2.2 The heuristic approach

It is well known[1-9] that axially-symmetric ideal nondiffracting pulses (INP) can be made by zero order Bessel beam superpositions,

$$\Psi(\rho, z, t) = \int_0^\infty d\omega \int_{-\omega/c}^{\omega/c} d\beta \bar{S}(\omega, \beta) J_0 \left( \rho \sqrt{\frac{\omega^2}{c^2} - \beta^2} \right) e^{i\beta z} e^{-i\omega t} \quad (4)$$

**provided that** the spectral function  $\bar{S}(\omega, \beta)$  entails a linear relationship of the type

$$\omega = V\beta + b \quad (5)$$

between  $\omega$  and  $\beta$ . In this way, by putting  $\bar{S}(\omega, \beta) = S(\omega)\delta(\omega - V\beta - b)$ , the general form of an axially-symmetric INP gets written as

$$\Psi_{INP}(\rho, z, t) = e^{-ibz/V} \int_{\omega_{min}}^{\omega_{max}} d\omega S(\omega) J_0 \left( \rho \sqrt{\left(\frac{1}{c^2} - \frac{1}{V^2}\right) \omega^2 + \frac{2b\omega}{V^2} - \frac{b^2}{V^2}} \right) e^{i\omega z/V} \quad (6)$$

where  $\zeta = z - Vt$ , and  $S(\omega)$  is the frequency spectrum. Obviously, the INP will be subluminal, luminal or supeluminal, depending on the value of  $V$ , it being  $<$ ,  $=$  or  $> c$ . The positive quantities  $\omega_{min}$  and  $\omega_{max}$  are the minimum and maximum angular frequency allowed for the Bessel beams in the superposition (6), and their values have to be estimated as follows.

Once we have chosen the value of  $V$  in (6), the values of  $b$ ,  $\omega_{min}$  and  $\omega_{max}$  are to related between them in such a way that

$$k_\rho^2 = \left(\frac{1}{c^2} - \frac{1}{V^2}\right)\omega^2 + \frac{2b\omega}{V^2} - \frac{b^2}{V^2} \geq 0 \quad (7)$$

$$\beta \geq 0$$

for all positive angular frequency  $\omega_{min} \leq \omega \leq \omega_{max}$  used in the superposition (6).

In relation (7), the condition on  $k_\rho$  eliminates any unphysical behaviors of Bessel functions and evanescent waves in Eq.(6). The second condition ( $\beta \geq 0$ ) eliminates any backwards-travelling Bessel beams in the same superposition, since we are considering positive values of the angular frequency only.

Taking into account conditions (7), one has:

- For Subluminal ( $V < c$ ) INPs:  $b > 0$ ,  $\omega_{min} = b$  and  $\omega_{max} = cb/(c - V)$
- For Luminal ( $V = c$ ) INPs:  $b > 0$ ,  $\omega_{min} = b$  and  $\omega_{max} = \infty$
- For Superluminal ( $V > c$ ) INPs:  $b \geq 0$ ,  $\omega_{min} = b$  and  $\omega_{max} = \infty$ . Or  $b < 0$ ,  $\omega_{min} = cb/(c - V)$  and  $\omega_{max} = \infty$

The INPs provided by Eq.(6) can propagate without distortion indefinitely, with peak-velocity  $V$ .

Such INPs possess an infinite energy, and so, for real applications, they must be spatially truncated (i.e., generated by finite apertures)[11-14], resulting in finite energy solutions, with a finite depth of field.

When such truncation is made, the resulting pulse in general cannot be obtained in an analytical form, but has to be numerically calculated from the diffraction theory, by using, for example, the Rayleigh-Sommerfeld formula[10-14]. That is, once we have a known INP solution  $\Psi_{INP}$ , its truncated version  $\Psi_{TNP}$ , generated by a finite aperture of radius  $R$  on the plane  $z = 0$ , results given by

$$\Psi_{TNP}(\rho, z, t) = \int_0^{2\pi} d\phi' \int_0^R d\rho' \rho' \frac{1}{2\pi D} \left\{ [\Psi] \frac{(z - z')}{D^2} + [\partial_{ct'} \Psi] \frac{(z - z')}{D} \right\} \quad (8)$$

the quantities enclosed by the square brackets being evaluated at the retarded time  $ct' = ct - D$ . The distance  $D = \sqrt{(z - z')^2 + \rho^2 + \rho'^2 - 2\rho\rho' \cos(\phi - \phi')}$  is the separation between the source and observation points.

Due to its complexity, Eq.(8) has to be solved numerically in most cases.

Of particular interest is the on-axis behavior of  $\Psi_{TNP}$ . Actually, many important information can be extracted from the evolution of  $\Psi_{TNP}(\rho = 0, z, t)$ , like its depth of field, the pulse decaying rate, its longitudinal behavior, the effects of the different spectral parameters on the pulse evolution; and, even more important, quantity  $\Psi_{TNP}(\rho = 0, z, t)$  can be used to compare the performance of different kinds of TNP, as for example, the luminal and the superluminal ones.

On considering axially-symmetric TNP, and making  $\rho = 0$  in Eq.(8), we get some simplifications, because the integration on  $\phi'$  can be immediately done: But, even in this case, the integration on  $\rho'$  rarely can be carried on analytically, due to the complexity of the integrand, and numerical simulations are once more required.

To overcome this problem, let us propose the following heuristic approach:

First, we consider the Bessel beam superposition (6), which provides us with the INPs.

Second, we make the assumption that each Bessel beam, with frequency  $\omega$  and axicon angle  $\theta(\omega)$ , entering in superposition (6), obeys the following condition:

$$R \gg \frac{1}{k_\rho} = \frac{c}{\omega \sin \theta(\omega)}, \quad (9)$$

$R$  being the radius of the finite aperture that will be used for truncating the INP.

The above assumption is very plausible, since efficient TNPs are generate by large apertures.

Once condition (9) is fulfilled by all Bessel beams in superposition (6), we can use again the geometrical optics and assume that, after the truncation, the on-axis behavior of each one of those Bessel beams can be approximated by Eq.(3).

Third, taking into account Eqs.(3) and (6), we may conjecture that the on-axis evolution of the *truncate* nondiffracting pulse is approximately given by:

$$\Psi_{TNP}(\rho = 0, z, t) \simeq e^{-ibz/V} \int_{\omega_{min}}^{\omega_{max}} d\omega S(\omega) e^{i\omega\zeta/V} \left[ H(z) - H\left(z - \frac{R}{\tan \theta(\omega)}\right) \right], \quad (10)$$

where  $H(\cdot)$  is the Heaviside step function and, let us recall,  $\theta(\omega)$  is the axicon angle of the Bessel beam with angular frequency  $\omega$ .

We should notice that in the integrand of (10), the step function  $H(z - R/\tan \theta(\omega))$  depends on  $\omega$ , through of  $\theta(\omega)$ .

We can rewrite Eq.(10) in the form

$$\begin{aligned} \Psi_{TNP}(\rho = 0, z > 0, t) \simeq & e^{-ibz/V} \left[ \int_{\omega_{min}}^{\omega_{max}} S(\omega) e^{i\omega\zeta/V} d\omega \right. \\ & \left. - \int_{\omega_{min}}^{\omega_{max}} S(\omega) e^{i\omega\zeta/V} H\left(z - \frac{R}{\tan \theta(\omega)}\right) d\omega \right] \end{aligned} \quad (11)$$

where the first term in the r.h.s. of (11) is nothing but the INP  $\Psi_{INP}(\rho = 0, z, t)$ , while the second term is the perturbation due to the truncation.



Now, remembering that for a Bessel beam of axicon angle  $\theta$  we have  $\omega = c\beta/\cos\theta$ , and that the spectra of INPs impose the constraint  $\omega = V\beta + b$  between angular frequencies and longitudinal wavenumbers, it becomes easy to show that

$$\frac{R}{\tan\theta(\omega)} = \frac{R}{\sqrt{1 - \left(\frac{c}{V} - \frac{bc}{V\omega}\right)^2}} \left(\frac{c}{V} - \frac{bc}{V\omega}\right) \quad (12)$$

and thus

$$\begin{aligned} H\left(z - \frac{R}{\tan\theta(\omega)}\right) &= H\left(z - \frac{R\left(\frac{c}{V} - \frac{bc}{V\omega}\right)}{\sqrt{1 - \left(\frac{c}{V} - \frac{bc}{V\omega}\right)^2}}\right) \\ &= \begin{cases} 1 & \text{for } z \geq \frac{R\left(\frac{c}{V} - \frac{bc}{V\omega}\right)}{\sqrt{1 - \left(\frac{c}{V} - \frac{bc}{V\omega}\right)^2}} \\ 0 & \text{for } z < \frac{R\left(\frac{c}{V} - \frac{bc}{V\omega}\right)}{\sqrt{1 - \left(\frac{c}{V} - \frac{bc}{V\omega}\right)^2}} \end{cases} \end{aligned} \quad (13)$$

With all what precedes, we can eventually write

$$\begin{aligned} \Psi_{TNP}(\rho = 0, z, t) &\simeq e^{-ibz/V} \left[ \int_{\omega_{min}}^{\omega_{max}} S(\omega) e^{i\omega\zeta/V} d\omega \right. \\ &\quad \left. - \int_{\omega_{min}}^{\omega_{max}} S(\omega) e^{i\omega\zeta/V} H\left(z - \frac{R\left(\frac{c}{V} - \frac{bc}{V\omega}\right)}{\sqrt{1 - \left(\frac{c}{V} - \frac{bc}{V\omega}\right)^2}}\right) d\omega \right] \end{aligned} \quad (14)$$

In the next subsection, we will analyze the fundamental Eq.(14) for the three possible types of TNPs: subluminal, luminal, and superluminal.

### 2.2.1 Subluminal TNP

For the subluminal pulses ( $V < c$ ), we have  $b > 0$ ,  $\omega_{min} = b$  and  $\omega_{max} = cb/(c - V)$ .

In this way, taking into account these facts, and that  $z \geq 0$  and  $\omega_{min} \leq \omega \leq \omega_{max}$ , we can show, after several manipulations, that Eq.(13) can be written as

$$H \left( z - \frac{R \left( \frac{c}{V} - \frac{bc}{V\omega} \right)}{\sqrt{1 - \left( \frac{c}{V} - \frac{bc}{V\omega} \right)^2}} \right) = \begin{cases} 1 & \text{for } \omega \leq \frac{bc}{c - \frac{zV}{\sqrt{z^2 + R^2}}} \\ 0 & \text{for } \omega > \frac{bc}{c - \frac{zV}{\sqrt{z^2 + R^2}}} \end{cases} \quad (15)$$

Now, by noting that  $\omega_{min} = b < bc/(c - zV/\sqrt{z^2 + R^2}) < \omega_{max} = bc/(c - V)$ , one can write Eq.(14), for the *subluminal* case, as

$$\begin{aligned} \Psi_{TNP}(\rho = 0, z > 0, t) &\simeq e^{-ibz/V} \left[ \int_b^{\frac{bc}{c-V}} S(\omega) e^{i\omega\zeta/V} d\omega - \int_b^{\frac{bc}{c - \frac{zV}{\sqrt{z^2 + R^2}}}} S(\omega) e^{i\omega\zeta/V} d\omega \right] \\ &= e^{-ibz/V} \left[ \int_{\frac{bc}{c - \frac{zV}{\sqrt{z^2 + R^2}}}}^{\frac{bc}{c-V}} S(\omega) e^{i\omega\zeta/V} d\omega \right], \end{aligned} \quad (16)$$

**which represents our method in the case of subluminal TNPs.** It is a very simple equation, capable of providing closed-form, analytical results for several different frequency spectra  $S(\omega)$ , as we shall see in Section 3.

### 2.2.2 Luminal TNP

For luminal TNPs ( $V = c$ ), we have  $b > 0$ ,  $\omega_{min} = b$  and  $\omega_{max} = \infty$ .

With this, and taking into account that  $z \geq 0$  and  $\omega_{min} \leq \omega \leq \omega_{max}$ , we can, after several manipulations, show that Eq.(13) may be written as

$$H \left( z - \frac{R \left( \frac{c}{V} - \frac{bc}{V\omega} \right)}{\sqrt{1 - \left( \frac{c}{V} - \frac{bc}{V\omega} \right)^2}} \right) = \begin{cases} 1 & \text{for } \omega \leq \frac{b}{1 - \frac{z}{\sqrt{z^2 + R^2}}} \\ 0 & \text{for } \omega > \frac{b}{1 - \frac{z}{\sqrt{z^2 + R^2}}} \end{cases}, \quad (17)$$

and, by noting that  $\omega_{min} = b < b/(1 - z/\sqrt{z^2 + R^2}) < \omega_{max} = \infty$ , we can write Eq.(14), for the *luminal* case, as

$$\begin{aligned} \Psi_{TNP}(\rho = 0, z > 0, t) &\simeq e^{-ibz/c} \left[ \int_b^\infty S(\omega) e^{i\omega\zeta/c} d\omega - \int_b^{\frac{b}{1 - \frac{z}{\sqrt{z^2 + R^2}}}} S(\omega) e^{i\omega\zeta/c} d\omega \right] \\ &= e^{-ibz/c} \left[ \int_{\frac{b}{1 - \frac{z}{\sqrt{z^2 + R^2}}}}^\infty S(\omega) e^{i\omega\zeta/c} d\omega \right], \end{aligned} \quad (18)$$

Equation (18), **which represents our method in the case of luminal TNPs**, is very simple too, and can provide closed-form, analytical results for many different frequency spectra  $S(\omega)$ , as we shall see in Section 3.

### 2.2.3 Superluminal TNP

For superluminal TNPs ( $V > c$ ), the value of  $b$ , in the the spectral constraint (5), can assume negative or positive values, i.e.,  $-\infty \leq b \leq \infty$ . Let us analyze the superluminal case of Eqs.(13) and (14) for both situations,  $b < 0$  and  $b \geq 0$ .

#### Superluminal case for $b < 0$

In this case, we have  $\omega_{min} = cb/(c - V)$  and  $\omega_{max} = \infty$ .

Taking into account that  $z \geq 0$  and  $\omega_{min} \leq \omega \leq \omega_{max}$ , and, again, after several manipulations, we can show that for this case Eq.(13) can be written as

$$H \left( z - \frac{R \left( \frac{c}{V} - \frac{bc}{V\omega} \right)}{\sqrt{1 - \left( \frac{c}{V} - \frac{bc}{V\omega} \right)^2}} \right) = \begin{cases} 1 & \text{for } \omega \leq \frac{bc}{c - \frac{zV}{\sqrt{z^2 + R^2}}} \text{ and } z \leq \frac{R}{\sqrt{V^2/c^2 - 1}} \\ 1 & \text{for } \omega \geq \frac{bc}{c - \frac{zV}{\sqrt{z^2 + R^2}}} \text{ and } z \geq \frac{R}{\sqrt{V^2/c^2 - 1}} \\ 0 & \text{otherwise} \end{cases} \quad (19)$$

By noting that, when  $z \leq R/\sqrt{V^2/c^2 - 1}$ , we have  $bc/(c - zV/\sqrt{z^2 + R^2}) \leq 0$  and that, when  $z \geq R/\sqrt{V^2/c^2 - 1}$ , we have  $bc/(c - zV/\sqrt{z^2 + R^2}) > \omega_{min} = bc/(c - V)$ , one can write Eq.(14), for the case  $V > c$  and  $b < 0$ , as

$$\Psi_{TNP}(\rho = 0, z > 0, t) \simeq \begin{cases} e^{-ibz/V} \int_{\frac{bc}{c-V}}^{\infty} S(\omega) e^{i\omega\zeta/V} d\omega & \text{for } z \leq \frac{R}{\sqrt{V^2/c^2 - 1}} \\ e^{-ibz/V} \int_{\frac{bc}{c-V}}^{\frac{bc}{c - \frac{zV}{\sqrt{z^2 + R^2}}}} S(\omega) e^{i\omega\zeta/V} d\omega & \text{for } z \geq \frac{R}{\sqrt{V^2/c^2 - 1}} \end{cases}, \quad (20)$$

Equation (18), represents our method in the case of superluminal TNPs with  $b < 0$ . Again, the integrals are very simple, and can provide closed-form, analytical results for many spectra  $S(\omega)$ .

Before going on to the next case, one can immediately see from Eq.(20) that, independently of  $S(\omega)$ , the superluminal TNPs with  $b < 0$  will reach the distance  $z = R/\sqrt{V^2/c^2 - 1}$  without deforming.

### Superluminal case for $b \geq 0$

In this case, we have  $\omega_{min} = b$  and  $\omega_{max} = \infty$ .

Remembering that  $z \geq 0$  and  $\omega_{min} \leq \omega \leq \omega_{max}$ , and, as before, after several manipulations, we can show that in this case Eq.(13) can be written in the same form of Eq.(19).

Now, taking into account that, when  $z \leq R/\sqrt{V^2/c^2 - 1}$ , it is  $\omega_{min} = b \leq bc/(c - zV/\sqrt{z^2 + R^2}) \leq \omega_{max} = \infty$  and that, when  $z > R/\sqrt{V^2/c^2 - 1}$ , one has  $bc/(c - zV/\sqrt{z^2 + R^2}) < 0$ , we can write our fundamental Eq.(14), for the case  $V > c$  and  $b \geq 0$ , in the form

$$\Psi_{TNP}(\rho = 0, z > 0, t) \simeq \begin{cases} e^{-ibz/V} \int_{\frac{bc}{c - \frac{zV}{\sqrt{z^2 + R^2}}}}^{\infty} S(\omega) e^{i\omega\zeta/V} d\omega & \text{for } z \leq \frac{R}{\sqrt{V^2/c^2 - 1}} \\ 0 & \text{for } z \geq \frac{R}{\sqrt{V^2/c^2 - 1}} \end{cases}, \quad (21)$$

Equation (18), **represents our method in the case of superluminal TNPs with  $b \geq 0$** . Again, many closed-form results, for many different spectra  $S(\omega)$ , can be obtained from the above equation.

We can also notice from Eq.(21) that, for  $V > c$  and  $b \geq 0$ , the superluminal TNPs will get very low intensities after the distance  $z = R/\sqrt{V^2/c^2 - 1}$ .

It is important to notice that in our method, given by Eqs.(16), (18), (20, 21), the on-

axis evolution of a TNP depends only on the frequency spectrum  $S(\omega)$  of its corresponding INP  $\Psi_{INP}$ , at variance with the Rayleigh-Sommerfeld formula (8), which depends on the mathematical expression of  $\Psi_{INP}$ .

Now, we shall go on to the next Section, where our method will be applied to some important kinds of localized waves, and our results will be compared with those obtained by making numerical simulations by the Rayleigh-Sommerfeld formula.

### 3 Application to some important cases. Closed-form, analytical results, and their comparison with numerical simulations of the Rayleigh-Sommerfeld formula.

The method we have developed in the previous Section is described by Eqs.(16), (18), (20, 21), for the cases of truncated subluminal, luminal and superluminal pulses, respectively.

We are going to apply, now, this method to some important cases involving TNPs; and it will be shown that the results agree very well with those obtained through numerical simulations of the Rayleigh-Sommerfeld formula (8).

#### 3.1 The method applied to a truncated subluminal pulse

A well known ideal subluminal ( $V < c$ ) nondiffracting pulse[20] is

$$\Psi_{INP}(\rho, z, t) = \exp\left(\frac{ibV\gamma^2\eta}{c^2}\right) \text{sinc}\left(\frac{b\gamma}{c}\sqrt{\rho^2 + \gamma^2\zeta^2}\right) \quad (22)$$

where  $\gamma = 1/\sqrt{1 - V^2/c^2}$ ,  $\eta = z - c^2t/V$  and, as always,  $\zeta = z - Vt$ .

Now, we want to describe the on-axis behavior of the *truncated* version ( $\Psi_{TNP}$ ) of the ideal solution (22).

The subluminal INP (22) is generated by the superposition (6), with a constant spectrum  $S(\omega) = c/(2bV\gamma^2)$ . However, we have to notice that this solution possesses backwards-travelling components: Actually, it has  $\omega_{min} = bc/(c+V)$ , instead of  $\omega_{min} = b$  (which assures forward components only in (6), as we have seen in Section 2). It is the price paid to get such a closed-form and exact INP solution.

Anyway, we may, and we must, minimize the contribution of those “backwards” components by choosing the subluminal velocity  $V$  in such a way that  $(c+V)/(c-V) \gg 1$ . Once this condition is satisfied, we can observe that the INP (22) is, then, similar to that which would be obtained with the same  $S(\omega)$ , but with  $\omega_{min} = b$ .

It should be noticed that the comments and observations above have nothing to do with our method, which is constructed since the beginning in order to comprehend causal (forward) solutions only, and can be used for any values of the velocity  $V$ . Those remarks were made just in order that a causal behavior of the INP (22) be guaranteed.

Now, on using  $S(\omega) = c/(2bV\gamma^2)$  in our Eq.(16), which describes the on-axis evolution of the subluminal TNPs, one gets

$$\begin{aligned} \Psi_{TNP}(\rho = 0, z > 0, t) &\simeq \frac{c}{2bV\gamma^2} e^{-ibz/V} \left[ \int_{\frac{bc}{c-V}}^{\frac{bc}{c-\frac{zV}{\sqrt{z^2+R^2}}}} e^{i\omega\zeta/V} d\omega \right] \\ &= \frac{cV}{2bV\gamma^2 i\zeta} e^{-ibz/V} \left[ \exp\left(\frac{ibc}{V(c-V)}\zeta\right) - \exp\left(\frac{ibc\sqrt{z^2+R^2}}{V(c\sqrt{z^2+R^2}-zV)}\zeta\right) \right], \end{aligned} \quad (23)$$

which is a very simple closed-form, analytical expression.

First, we use Eq.(23) to get the pulse-peak intensity behavior. To do this, we just put  $z = Vt \rightarrow \zeta = 0$  in (23).

Let us consider three different cases: (1)  $V = 0.995c$  and  $b = 1.5 \times 10^{15}\text{Hz}$ ; (2)

$V = 0.998c$  and  $b = 6 \times 10^{14}\text{Hz}$ , and (3)  $V = 0.9992c$  and  $b = 2.4 \times 10^{14}\text{Hz}$ . In all cases, we consider the radius of the finite aperture to be  $R = 4$  mm.

At the same time, we compare our result with that obtained by the numerical simulation of the Rayleigh-Sommerfeld formula (8), with  $\Psi_{INP}$  given by (22).

Figure 2 shows the plots, where those represented by continuous lines have been obtained from our equation (23), while those represented by dotted lines come from the numerical simulation of (8).

We can verify the excellent agreement existing among those results.

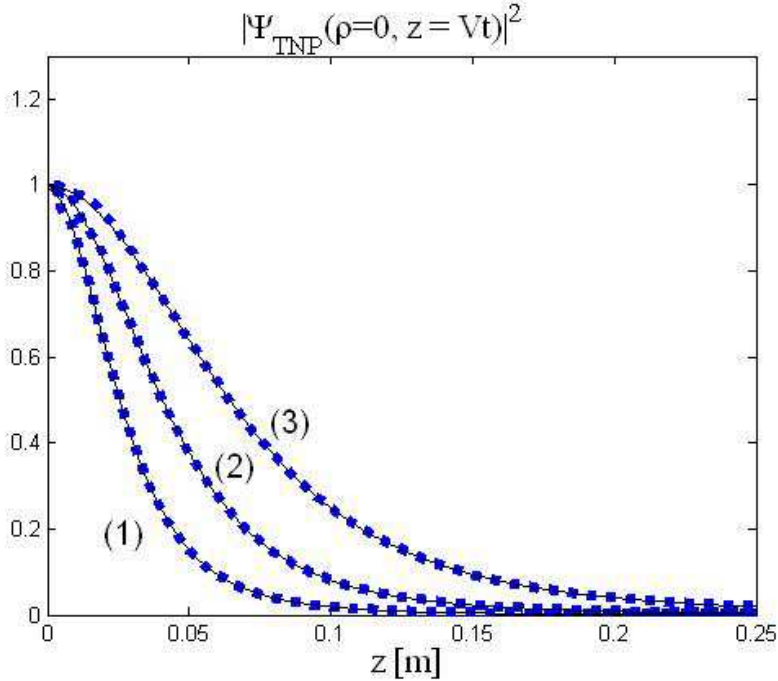


Figure 2: The peak intensity evolution of this subluminal TNP for the three cases: (1)  $V = 0.995c$  and  $b = 1.5 \times 10^{15}\text{Hz}$ . (2)  $V = 0.998c$  and  $b = 6 \times 10^{14}\text{Hz}$ . (3)  $V = 0.9992c$  and  $b = 2.4 \times 10^{14}\text{Hz}$ . In all cases  $R = 4$  mm. The continuous lines are obtained from our closed-form analytical expression (23) and those represented by dotted lines come from the numerical simulation of the Rayleigh-Sommerfeld formula (8).



Now, we are interested in the on-axis longitudinal pulse evolution, in the three cases above considered, in the time instants given by  $t' = 0.11$  ns,  $t'' = 0.22$  ns and  $t''' = 0.33$  ns.

Figures (3a,3b,3c) show the results corresponding to the cases (1), (2) and (3), respectively. As before, the continuous lines represent the results obtained from our Eq.(23), and the dotted ones those coming from the numerical simulation of (8). Again, we consider  $R = 4$  mm.

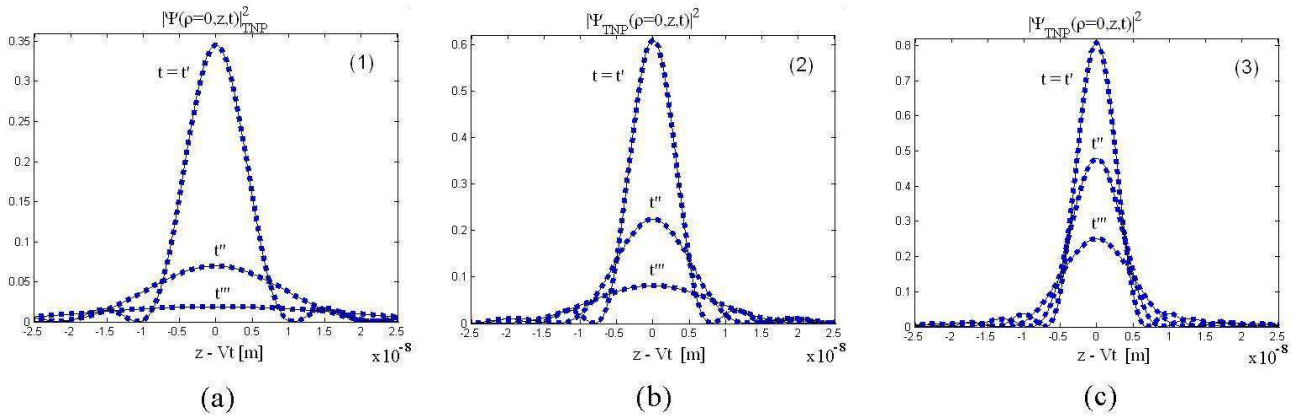


Figure 3: The on-axis evolution of this subluminal TNP, in the times  $t' = 0.11$ ns,  $t'' = 0.22$ ns and  $t''' = 0.33$ ns, for each case cited in Fig.2. Figure 3a, 3b and 3c represent the cases (1),(2) and (3) respectively. The continuous lines are the results obtained from our closed-form analytical expression (23) and those represented by dotted lines come from the numerical simulation of the Rayleigh-Sommerfeld formula (8).

We can observe, once more, a very good agreement among the results, confirming that our method works very well.

### 3.2 The method applied to the truncated luminal Focus Wave Mode pulse

A very famous ideal luminal ( $V = c$ ) nondiffracting pulse[1] is the Focus Wave Mode pulse (FWM), given by

$$\Psi_{INP}(\rho, z, t) = \frac{ac}{ac - i\zeta} \exp\left(\frac{-ib}{2c}\eta\right) \exp\left(\frac{-b\rho^2}{2c(ac - i\zeta)}\right), \quad (24)$$

where  $\eta = z + ct$ ,  $\zeta = z - ct$ , and  $a > 0$  is a constant.

Like all the INPs, the FWM possesses infinite energy and must be truncated (i.e., generated by a finite aperture) for real applications. We shall use our method to get closed-form, analytical expressions for the on-axis evolution of the truncated version  $\Psi_{TNP}$  of Eq.(24).

The exact ideal solution (24) is obtained from the superposition (6) with  $V = c$  and  $S(\omega) = a\exp(ab/2)\exp(-a\omega)$ . Because it has  $\omega_{min} = b/2$ , instead of  $\omega_{min} = b$ , its spectrum possesses backwards components[1-6] in the range  $b/2 \leq \omega < b$ . To overcome this problem, we must minimize the contribution of the nonphysical part of the spectrum; and this can be done if  $ab \ll 1$ . Once such a condition is obeyed, the INP (24) can be considered similar to the one that we would obtain with the same frequency spectrum of the FWM, but with  $\omega_{min} = b$ .

Again, let us notice that such remarks are made just to validate the causality of the INP (24), and have nothing to do with our own method.

Now, by using  $S(\omega) = a\exp(ab/2)\exp(-a\omega)$  in our Eq.(18), we get the on-axis evolution of the truncated FWM:

$$\begin{aligned} \Psi_{TNP}(\rho = 0, z > 0, t) &\simeq ae^{ab/2}e^{-ibz/c} \int_{\frac{b}{1 - \frac{z}{\sqrt{z^2 + R^2}}}}^{\infty} e^{-a\omega} e^{i\omega\zeta/c} d\omega \\ &= \frac{ac}{ac - i\zeta} e^{ab/2} e^{-ibz/c} \exp\left(\frac{-b\sqrt{z^2 + R^2}(ac - i\zeta)}{c(\sqrt{z^2 + R^2} - z)}\right), \end{aligned} \quad (25)$$

which is a very simple closed-form, analytical expression.

First, let us put  $\zeta = 0$  in our Eq.(25) in order to get the pulse-peak intensity behavior.

We consider three different cases: (1)  $a = 1.6 \times 10^{-16}$  and  $b = 5 \times 10^{11}$ Hz; (2)  $a = 1.25 \times 10^{-16}$ s and  $b = 3 \times 10^{11}$ Hz; and (3)  $a = 1 \times 10^{-16}$  and  $b = 2 \times 10^{11}$ Hz. In all cases we adopt the aperture radius  $R = 2$  mm.

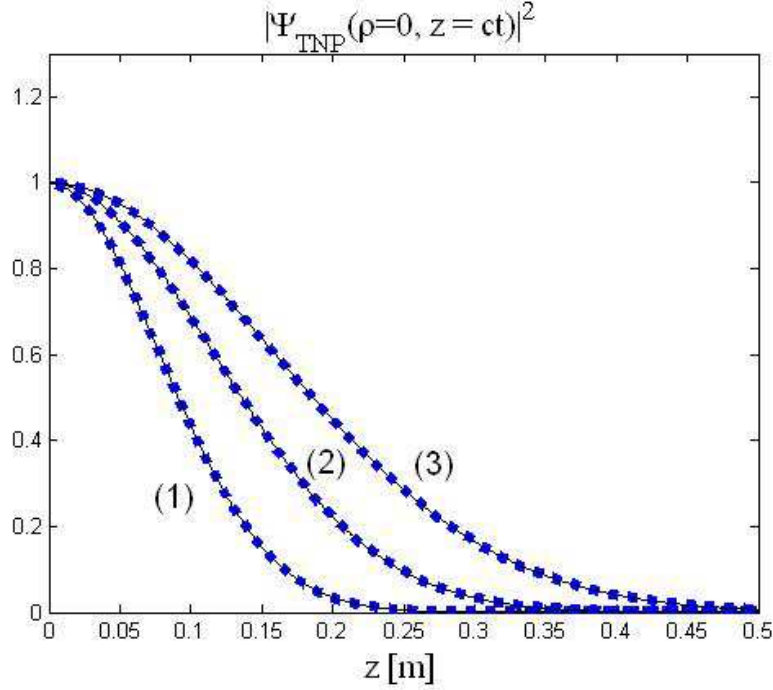


Figure 4: The peak-intensity evolution of the truncated luminal FWM pulse for the three cases: (1)  $a = 1.6 \times 10^{-16}$  and  $b = 5 \times 10^{11}$ Hz; (2)  $a = 1.25 \times 10^{-16}$ s and  $b = 3 \times 10^{11}$ Hz; (3)  $a = 1 \times 10^{-16}$  and  $b = 2 \times 10^{11}$ Hz. In all cases  $R = 2$  mm. The continuous lines are obtained from our closed-form analytical expression (25) and those represented by dotted lines come from the numerical simulation of the Rayleigh-Sommerfeld formula (8).

Figure 4 shows the results. The continuous lines represent the results obtained from our Eq.(25), while the dotted ones are the results of the numerical simulation of the Rayleigh-Sommerfeld formula (8).

The results agree so well, that the corresponding continuous and dotted curves do superpose to each other.

Now, we are going to use our Eq.(25) to show the on-axis evolution of this TNP, in

the three cases above considered, for the time instants  $t' = 0.22$  ns,  $t'' = 0.44$  ns and  $t''' = 0.66$  ns.

Figures (5a,5b,5c) show the results corresponding to the cases (1), (2) and (3), respectively. The continuous lines are the results obtained from our Eq.(25), and the dotted lines those coming from the numerical simulation of (8). Again, we consider  $R = 2$  mm.

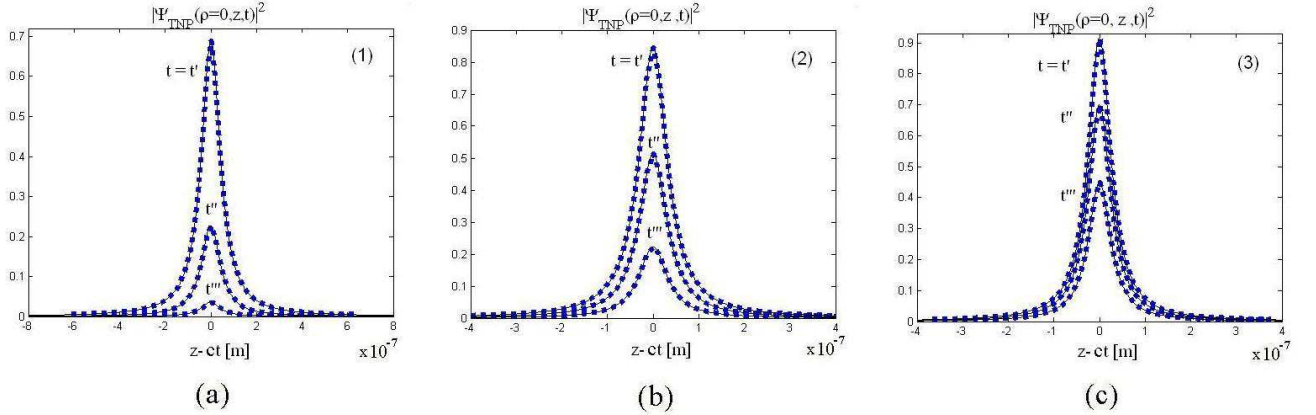


Figure 5: The on-axis evolution of the truncated luminal FWM pulse, at the times  $t' = 0.22$  ns,  $t'' = 0.44$  ns and  $t''' = 0.66$  ns, for each one of the cases cited in Fig.4. Figures 5a, 5b and 5c represent the cases (1),(2) and (3), respectively. The continuous lines are the results obtained from our closed-form analytical expression (25), while those represented by dotted lines come from the numerical simulation of the Rayleigh-Sommerfeld formula (8).

The results are in excellent agreement, showing the very good efficiency of the method.

### 3.3 The method applied to the truncated Superluminal Focus Wave Mode pulse

An interesting, approximated, superluminal ( $V > c$ ) ideal nondiffracting solution to the wave equation is the so-called[6] Superluminal Focus Wave Mode pulse (SFWM):

$$\Psi_{INP}(\rho, z, t) = aV \exp\left(\frac{-ib}{2V}\eta\right) X \exp\left(\frac{b(V^2 + c^2)}{2V(V^2 - c^2)} \left((aV - i\zeta) - X^{-1}\right)\right), \quad (26)$$

where  $\eta = z + Vt$ ,  $\zeta = z - Vt$ ,  $a > 0$  is a constant, and where

$$X = \left( (aV - i\zeta)^2 + \left( \frac{V^2}{c^2} - 1 \right) \rho^2 \right)^{-1/2} \quad (27)$$

Expression (21) is a very good approximate solution of the wave equation[6] if  $ab \ll 1$ , which is also the condition for minimizing the contribution of the backwards components of (21). Actually, this superluminal INP can be obtained from superposition (6), with  $b > 0$ , when using  $S(\omega) = a \exp(ab/2) \exp(-a\omega)$ , with constant  $a > 0$ , but with  $\omega_{min} = b/2$  instead of  $\omega_{min} = b$ .

To get the closed-form, analytical mathematical expression that describes the on-axis evolution of the truncated version of (26), let us put  $S(\omega) = a \exp(ab/2) \exp(-a\omega)$  in our Eq.(21):

$$\Psi_{TNP}(\rho = 0, z > 0, t) \simeq \begin{cases} \frac{aV e^{ab/2} e^{-ibz/V}}{aV - i\zeta} \exp\left( \frac{-bc\sqrt{z^2 + R^2} (aV - i\zeta)}{V(c\sqrt{z^2 + R^2} - zV)} \right) & \text{for } z \leq \frac{R}{\sqrt{V^2/c^2 - 1}} \\ 0 & \text{for } z \geq \frac{R}{\sqrt{V^2/c^2 - 1}} \end{cases}, \quad (28)$$

Now, let us set  $\zeta = 0$  in our Eq.(28), for analyzing the peak-intensity behavior of the truncated SFWM.

We consider three different cases: (1)  $V = 1.0002 c$ ,  $b = 3 \times 10^{12}$ Hz and  $a = 2.5 \times 10^{-17}$ s; (2)  $V = 1.0001 c$ ,  $b = 1 \times 10^{12}$ Hz and  $a = 5 \times 10^{-17}$ s; and (3)  $V = 1.00008 c$ ,  $b = 2 \times 10^{12}$ Hz and  $a = 1.1 \times 10^{-17}$ s. In all these cases we choose  $R = 3$  mm as being the radius of the aperture.

The plots are shown in Fig.6, where the continuous lines represent our results using Eq.(28), and the dotted ones represent those obtained from the numerical simulation of

the Rayleigh-Sommerfeld formula (8). We can observe an excellent agreement among the results.

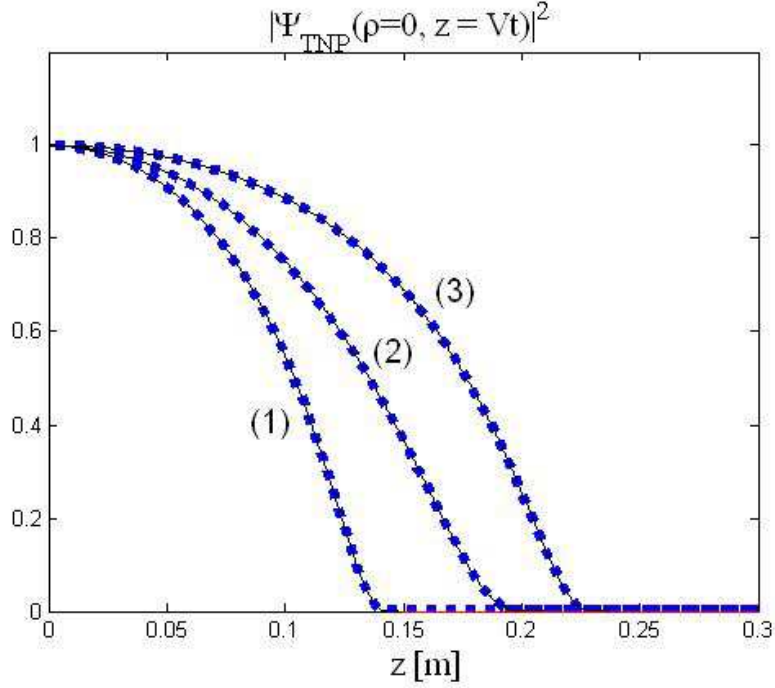


Figure 6: The peak intensity evolution of the truncated superluminal Focus Wave Mode pulse for the three cases: (1)  $V = 1.0002 c$ ,  $b = 3 \times 10^{12}\text{Hz}$  and  $a = 2.5 \times 10^{-17}\text{s}$ ; (2)  $V = 1.0001 c$ ,  $b = 1 \times 10^{12}\text{Hz}$  and  $a = 5 \times 10^{-17}\text{s}$ ; and (3)  $V = 1.00008 c$ ,  $b = 2 \times 10^{12}\text{Hz}$  and  $a = 1.1 \times 10^{-17}\text{s}$ . In all cases  $R = 3 \text{ mm}$ . The continuous lines are obtained from our closed-form, analytical expression (28), while those represented by dotted lines come from the numerical simulation of the Rayleigh-Sommerfeld formula (8)

Now, we are going to use our method to show the on-axis evolution of the pulse intensity at three different times  $t' = 0.14 \text{ ns}$ ,  $t'' = 0.29 \text{ ns}$  and  $t''' = 0.43 \text{ ns}$ , for each one of the cases cited above.

Figures (7a,7b,7c) show the plots. Again, the curves given by continuous lines come from our Eq.(28), while the dotted ones from the numerical simulation of (8).

Once more, there is an excellent agreement among the results, confirming the validity and efficiency of our method.

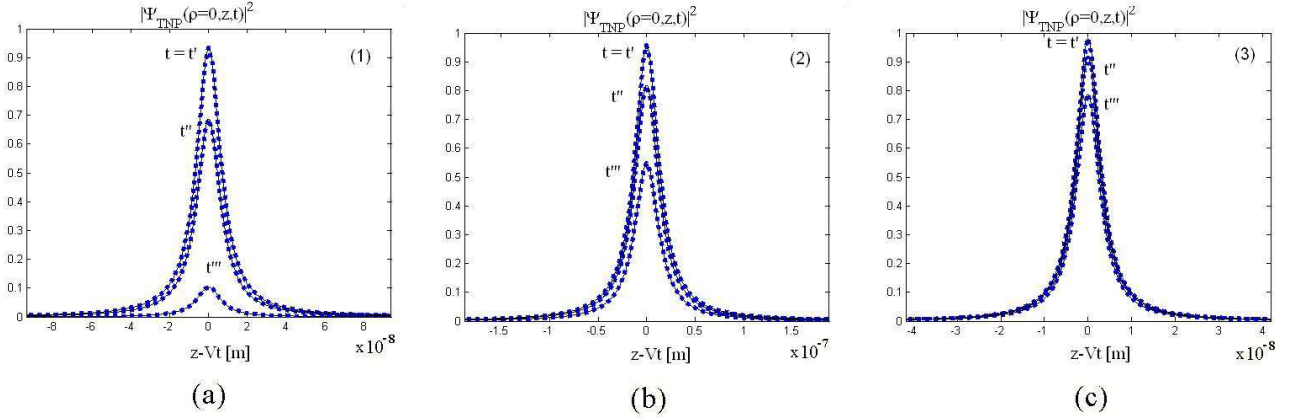


Figure 7: The on-axis evolution of the truncated SFWM pulse, at the times  $t' = 0.14$  ns,  $t'' = 0.29$  ns and  $t''' = 0.43$  ns, for each one of the cases cited in Fig.6. Figures 6a, 6b and 6c represent the cases (1),(2) and (3), respectively. The continuous lines are the results obtained from our closed-form, analytical expression (28), and those represented by dotted lines come from the numerical simulation of the Rayleigh-Sommerfeld formula (8).

## 4 Extending the present method to the almost non-diffracting (finite energy) pulses, truncated by finite apertures

In the previous Sections we have developed a (heuristic) method capable of providing closed-form analytical expressions, describing the on-axis evolution of the INP truncated by finite apertures.

It is well known[1,6] that, besides the INPs, there are the almost nondiffracting pulses (ANP), which also need infinite apertures to be generated, *but* possess a finite energy content.

Once a function  $S(\omega)$  is chosen, and an INP with a velocity  $V$  and  $b = b_0$  is obtained from Eq.(6), we can get an ANP by integrating Eq.(6), over the parameter  $b$ , with a

suitable choice of the weight function  $S'(b)$  which has to be concentrated around  $b = b_0$ .

More explicitly:

$$\Psi_{ANP}(\rho, z, t) = \int_{b_{min}}^{b_{max}} db \int_{\omega_{min}}^{\omega_{max}} d\omega S''(\omega, b) J_0 \left( \rho \sqrt{\left(\frac{1}{c^2} - \frac{1}{V^2}\right) \omega^2 + \frac{2b\omega}{V^2} - \frac{b^2}{V^2}} \right) e^{i\omega z/V} e^{-ibz/V}, \quad (29)$$

where  $S''(\omega, b) = S(\omega)S'(b)$  is a spectral function with  $S'(b)$  well localized around  $b = b_0$ .

Obviously, one can recover the INPs just by adopting the choice  $S''(\omega, b) = S(\omega)\delta(b - b_0)$ .

An ANP can be viewed as a Bessel beam superposition (4) with a spectral function  $\bar{S}(\omega, \beta)$  well concentrated around a straight line  $\omega = V\beta + b_0$ .

The ANPs are interesting solutions, due to their finite energy contents, and can maintain their spatial shape for long distances[1,6].

However, even possessing finite energy, the ANPs need —as we were saying— infinite apertures to be generated: something that cannot be obtained in the real world. Due to this fact, it is rather important to know the behavior of these pulses when truncated by finite apertures; that is, to know the  $\Psi_{TNP_s}$  versions of the  $\Psi_{ANP_s}$ . This can be got by making numerical simulations, again, of the Rayleigh-Sommerfeld integral formula (8), on replacing  $\Psi_{INP}$  with  $\Psi_{ANP}$ .

**On the other hand, the extension of our method to the cases of ANPs truncated by finite apertures can be performed in a very simple way, just by multiplying our fundamental equations (16), (18) and (20, 21) by the  $S(b)$  under consideration, and performing the relevant integration over the parameter  $b$ .**

We are going to show this by the following example, in which we shall obtain closed-form analytical expressions for the truncated version  $\Psi_{TNP}$  with a well known finite energy



ANP[1,20]: Namely, the Modified Power Spectrum pulse (MPS).

*Example:* The truncated version of the MPS pulse.

A well-known luminal ANP is the MPS pulse, which can be obtained by integrating, over the parameter  $b$ , the FWM pulse (24) with the weight function

$$S'(b) = H(b - b_0) q \exp(-q(b - b_0)) , \quad (30)$$

quantities  $q$  and  $b_0$  being positive constants. More explicitly, the MPS pulse can be written as:

$$\begin{aligned} \Psi_{ANP}(\rho, z, t) &= \int_{b_0}^{\infty} \frac{aqc}{ac - i\zeta} \exp\left(\frac{-ib}{2c}\eta\right) \exp\left(\frac{-b\rho^2}{2c(ac - i\zeta)}\right) \exp(-q(b - b_0)) db \\ &= \frac{2ac^2q}{(2cq + i\eta)(ac - i\zeta) + \rho^2} \exp\left(\frac{-ib_0}{2c}\eta\right) \exp\left(-\frac{b_0\rho^2}{2c(ac - i\zeta)}\right) , \end{aligned} \quad (31)$$

with  $\eta = z + ct$ ,  $\zeta = z - ct$ .

This ANP has a finite energy content; however, it needs an infinite aperture to be generated.

We shall use the extended version of our method to get a closed-form analytical expression for the on-axis evolution of the truncated version,  $\Psi_{TNP}$ , of the MPS pulse. As we have seen, to get this we just need multiplying the truncated version of the FWM pulse, given by Eq.(25), by the corresponding weight function  $S'(b)$  given by (30), and performing the integration over the parameter  $b$ . In this way, the on-axis evolution of the truncated MPS pulse is given by:

$$\begin{aligned}
\Psi_{TNP}(\rho = 0, z > 0, t) &\simeq \int_{b_0}^{\infty} \frac{aqc}{ac - i\zeta} e^{ab/2} e^{-ibz/c} \exp(-q(b - b_0)) \exp\left(\frac{-b\sqrt{z^2 + R^2}(ac - i\zeta)}{c(\sqrt{z^2 + R^2} - z)}\right) db \\
&= \frac{aqc e^{ab_0/2} e^{-ib_0z/c}}{(ac - i\zeta) \left( q - \frac{a}{2} + \frac{iz}{c} + \frac{\sqrt{z^2 + R^2}(ac - i\zeta)}{c(\sqrt{z^2 + R^2} - z)} \right)} \exp\left(-\frac{b_0\sqrt{z^2 + R^2}(ac - i\zeta)}{c(\sqrt{z^2 + R^2} - z)}\right),
\end{aligned} \tag{32}$$

which is a closed-form analytical expression.

As before, let us put  $\zeta = 0$  in our Eq.(32) in order to get the pulse peak intensity behavior.

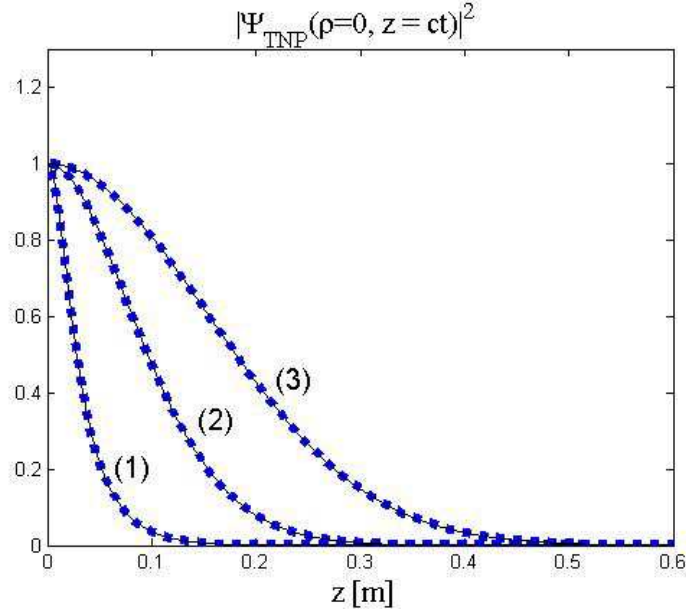


Figure 8: The peak-intensity evolution of the truncated luminal MPS pulse for the three cases: (1)  $a = 1.6 \times 10^{-16}$ ,  $b_0 = 5 \times 10^{11}$ Hz and  $q = 2 \times 10^{-11}$ s; (2)  $a = 1.25 \times 10^{-16}$ s,  $b_0 = 3 \times 10^{11}$ Hz and  $q = 10 \times 10^{-11}$ s; and (3)  $a = 1 \times 10^{-16}$ ,  $b_0 = 2 \times 10^{11}$ Hz and  $q = 20 \times 10^{-11}$ s. In all cases  $R = 2$  mm. The continuous lines are obtained from our closed-form analytical expression (32), while those represented by dotted lines come from the numerical simulation of the Rayleigh-Sommerfeld formula (8).

Let us consider three different cases: (1)  $a = 1.6 \times 10^{-16}$  s,  $b_0 = 5 \times 10^{11}$  Hz and  $q = 2 \times 10^{-11}$  s; (2)  $a = 1.25 \times 10^{-16}$  s,  $b_0 = 3 \times 10^{11}$  Hz and  $q = 10 \times 10^{-11}$  s; and (3)  $a = 1 \times 10^{-16}$  s,  $b_0 = 2 \times 10^{11}$  Hz and  $q = 20 \times 10^{-11}$  s. In all cases, we adopt the aperture radius  $R = 2$  mm.

Figure 8 shows the results. The continuous lines represent those obtained from our Eq.(32), while the dotted ones are the results of the numerical simulation of the Rayleigh-Sommerfeld integral formula (8).

One can verify the excellent agreement among the results.

Now, we are going to use our Eq.(32) to investigate the on-axis evolution of this TNP in the three cases above considered, for the instants  $t' = 0.22$  ns,  $t'' = 0.44$  ns and  $t''' = 0.66$  ns.

Figures (9a,9b,9c) show the results corresponding to the cases (1), (2) and (3), respectively. The continuous lines come from our Eq.(32), while the dotted lines are those coming from the numerical simulation of (8). Again, we consider  $R = 2$  mm.

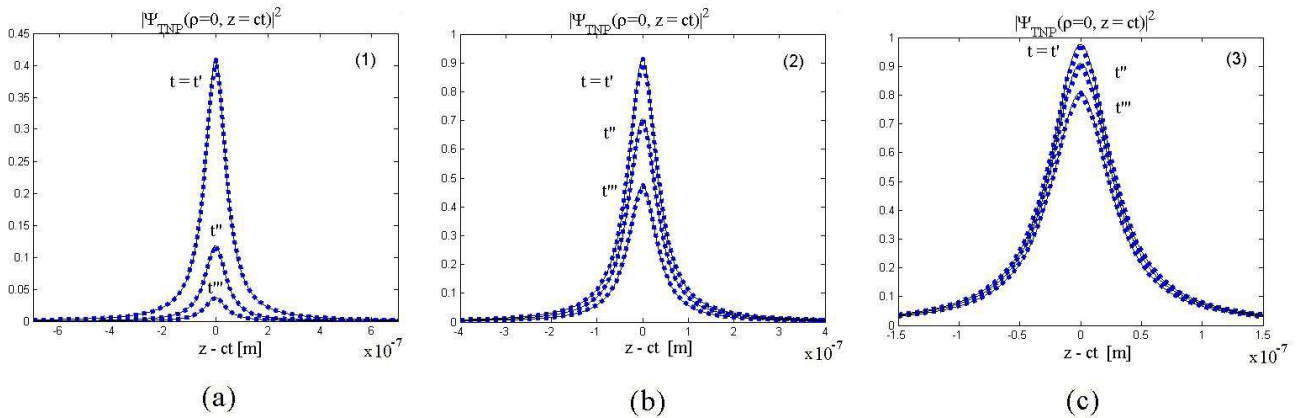


Figure 9: The on-axis evolution of the truncated luminal MPS pulse, at the times  $t' = 0.22$  ns,  $t'' = 0.44$  ns and  $t''' = 0.66$  ns, for each one of the three cases considered in Fig.8. Figures 9a, 9b and 9c represent the cases (1),(2) and (3), respectively. The continuous lines are the results obtained from our closed-form analytical expression (32), while those represented by dotted lines come from the numerical simulation of the Rayleigh-Sommerfeld formula (8).

Once more, there is an excellent agreement among the results, confirming the validity and efficiency of our method.

Before finishing this Section, it is important to notice that the closed-form analytical expressions of the truncated ANP, obtained with our method, can be advantageously used for comparison purposes with the corresponding non-truncated ANP: thus illustrating the effects due to the truncation, and, for example, telling us till what distance we can use the 3D solution of the ANP as a good approximation to the corresponding 3D TNP.

## 5 Conclusions

In this paper we have developed a very simple method for describing the space-time on-axis evolution of truncated nondiffracting pulses, be they subluminal, luminal or superluminal.

It is important to notice that in our method, given by Eqs.(16), (18), and (20, 21), the on-axis evolution of a TNP depends only on the frequency spectrum  $S(\omega)$  of its corresponding INP  $\Psi_{INP}$ , contrary to the Rayleigh-Sommerfeld formula (8) which depends on the explicit mathematical expression of  $\Psi_{INP}$ . We also have extended our method to describe the truncated versions of the ANPs.

Due to such a simplicity, we can obtain closed-form analytical expressions, which describing the on-axis evolution of innumerable TNPs. In this paper we have done that for the truncated versions of a few, very well-known, localized waves: subluminal, luminal, or superluminal.

We have compared our results with those obtained through the numerical simulation of the Rayleigh-Sommerfeld integrals, and we have observed an excellent agreement among them, confirming the efficiency of our method.

The present approach can be very useful, because it furnishes, in general, closed-form analytical expressions, avoiding the need of time-consuming numerical simulations; and

also because such expressions provide a powerful tool for exploring several important properties of the truncated localized pulses: as their depth of field, the longitudinal pulse behavior, the decaying rates, etc.

## 6 Acknowledgements

The author is very grateful to Erasmo Recami, Hugo E. Hernández-Figueroa and Claudio Conti for continuous discussions and kind collaboration. Thanks are also due to Jane M. Madureira.

This work was supported by FAPESP (Brazil).

E-mail address: mzamboni@dmo.fee.unicamp.br

## 7 References

- [1] I.M.Besieris, A.M.Shaarawi and R.W.Ziolkowski, “A bi-directional traveling plane wave representation of exact solutions of the scalar wave equation”, *J. Math. Phys.*, vol.30, pp.1254-1269, June 1989.
- [2] J.-y.Lu and J.F.Greenleaf, “Nondiffracting X-waves: Exact solutions to free-space scalar wave equation and their finite aperture realizations”, *IEEE Trans. Ultrason. Ferroelectr. Freq. Control*, vol.39, pp.19-31, Jan.1992.
- [3] J.Fagerholm, A.T.Friberg, J.Huttunen, D.P.Morgan and M.M.Salomaa, “Angular-spectrum representation of nondiffracting X waves”, *Phys. Rev., E*, vol.54, pp.4347-4352,

Oct.1996.

[4] P.Saari and K.Reivelt, "Evidence of X-shaped propagation-invariant localized light waves", *Phys. Rev. Lett.*, vol.79, pp.4135-4138, Nov.1997.

[5] E.Recami, "On localized X-shaped Superluminal solutions to Maxwell equations", *Physica A*, vol.252, pp.586-610, Apr.1998.

[6] M.Zamboni-Rached, E.Recami and H.E.Hernández F., "New localized Superluminal solutions to the wave equations with finite total energies and arbitrary frequencies," *Eur. Phys. J., D*, vol.21, pp.217-228, Sept.2002.

[7] M.A.Porras, S.Trillo, C.Conti and P.Di Trapani, "Paraxial envelope X-waves," *Opt. Lett.*, vol.28, pp.1090-1092, July 2003.

[8] G. Nyitray and S. V. Kukhlevsky, "Distortion-free tight confinement and step-like decay of fs pulses in free space", arXiv:physics/0310057 v1 13 Oct 2003.

[9] M. Zamboni-Rached, H.E. Hernandez-Figueroa, E. Recami "Chirped Optical X-type Pulses," *J. Opt. Soc. Am. A*, Vol. 21, pp. 2455-2463 (2004).

[10] Goodman J W, "Introduction to Fourier Optics", 1968 (New York: McGraw-Hill).

[11] R.W.Ziolkowski, I.M.Besieris and A.M.Shaarawi, "Aperture realizations of exact solutions to homogeneous wave-equations", *J. Opt. Soc. Am., A*, vol.10, pp.75-87, Jan.1993.

- [12] J.-y.Lu and J.F.Greenleaf, "Experimental verification of nondiffracting X-waves", *IEEE Trans. Ultrason. Ferroelectr. Freq. Control*, vol.39, pp.441-446, May 1992.
- [13] J.-y.Lu, H.-h.Zou and J.F.Greenleaf, "Biomedical ultrasound beam forming", *Ultrasound in Medicine and Biology*, vol.20, pp.403-428, 1994.
- [14] M. Zamboni-Rached, A. Shaarawi, E. Recami, "Focused X-Shaped Pulses", *Journal of Optical Society of America A*, Vol. 21, pp. 1564-1574 (2004).
- [15] J. Durnin, J. J. Miceli and J. H. Eberly, "Diffraction-free beams," *Phys. Rev. Lett.*, Vol. 58, pp. 1499-1501 (1987).
- [16] M. Zamboni-Rached, "Stationary optical wave fields with arbitrary longitudinal shape by superposing equal frequency Bessel beams: Frozen Waves", *Optics Express*, Vol. 12, pp.4001-4006 (2004).
- [17] M. Zamboni-Rached, E. Recami, H. Figueroa, "Theory of Frozen Waves: Modelling the Shape of Stationary Wave Fields", *J. Opt. Soc. Am. A*, Vol. 22, pp. 2465-2475 (2005).
- [18] M. Zamboni-Rached, "Diffraction-Attenuation Resistant Beams in Absorbing Media", arXiv:physics/0506067 v2 15 Jun 2005.
- [19] S. V. Kukhlevsky, M. Mechler, "Diffraction-free sub-wavelength beam optics at nanometer scale", *Opt. Comm.*, Vol. 231, pp. 35-43 (2004).

[20] R. Donnelly and R. W. Ziolkowski, “Designing localized waves”, Proc. R. Soc. Lond. A, Vol.440, pp.541-565 (1993).